

Chapter 18

Molecular Dynamics Simulations of Nanoparticles and Surfactants at Oil/Water Interfaces

A Qualitative Overview

R. J. K. Udayana Ranatunga,¹ Chuong T. Nguyen,¹ Chi-cheng Chiu,¹ Wataru Shinoda,² and Steven O. Nielsen^{*,1}

¹Department of Chemistry, University of Texas at Dallas, 800 West Campbell Road, Richardson, TX 75080

²Nanosystem Research Institute, National Institute of Advanced Industrial Science and Technology (AIST), 1-1-1 Umezono, Tsukuba, Ibaraki 305-8568, Japan

*steven.nielsen@utdallas.edu

Nanoparticles (NPs) and molecular surfactants are two classes of compounds which spontaneously localize at oil/water interfaces. Industrial and commercial applications of these systems often require precise two-dimensional organization of the localized NPs. An impediment to the realization of such systems is our under-developed understanding of the physics which governs the behavior of NPs in the presence of surfactants. Here we present a range of molecular dynamics simulation studies on non-ionic NP/surfactant systems. Analysis of the results allows us to relate the dispersive interactions of the NPs and surfactants to their physical behavior at oil/water interfaces.

Introduction

Documented study of the interfacial behavior of small colloidal particles began over a century ago, when Pickering (1) and Ramsden (2) separately investigated the spontaneous adsorption of colloidal particles to fluid interfaces (3). Since then the affinity of colloids to localize at fluid interfaces has been

harnessed in a number of fields (4). The interfacial activity of molecular surfactants, on the other hand, has been known for far longer. For example, historical evidence suggests that surfactants have been used for over 3500 years in the production of soap (5).

Recently, interest has arisen in systems containing both colloids and surfactants (6, 7). Advances in synthetic technology have resulted in the production of particles with progressively smaller sizes, unlocking the unique properties which emerge due to quantum confinement (8–10). Developments in methodology have also narrowed the size distribution of synthesized particles, greatly improving the aggregate properties and the reproducibility of systems composed of these nano-scaled particles. Many current and proposed applications of nanoparticles (NPs) involve systems of oil and water which also contain surfactants as emulsifiers. Therefore, given the propensity of NPs to localize at fluid interfaces it is important to understand the behavior of NPs and surfactants in the presence of one another.

In this chapter we focus on non-ionic surfactants and uncharged NPs at oil/water interfaces, studied through molecular dynamics (MD) computer simulations. The high spatial and temporal resolution of the MD trajectories facilitates a thorough examination of the interactions between the system components, and statistical mechanics provides us with a path to evaluate thermodynamic properties. A multi-pronged approach is used whereby several simulation schemes are carried out, each corresponding to a separate avenue of investigation, the results of which are presented in three sections:

- Unfunctionalized NPs at oil/water interfaces. Simulation results of individual NPs and groups of NPs are presented.
- Surfactants and NPs at oil/water interfaces. Simulations are presented of NPs in the presence of free surfactants. The cooperative behavior of the system components in lowering the oil/water interfacial tension is explored.
- Surfactant functionalized NPs at oil/water interfaces. Simulations are presented of NPs in the presence of chemically adsorbed surfactant ligands. The implication of the ‘softness’ that these coatings introduce to the composite particle is examined.

System Components and Simulation Details

Four components are essential for this study, namely nanoparticles, surfactants, water and oil. The choice of studying non-ionic species was taken because of the many advantages that these species present. The first of these advantages is that non-ionic surfactant-stabilized colloidal aggregates are known to be more robust than systems stabilized through electrostatic repulsion (11). Second, the dominant role that electrostatics plays in systems of large particles is mitigated at the nanoscale, and other factors such as dispersion interactions, entropy and steric interactions play equally important roles in determining the physical behavior of these systems (12). Apart from these reasons, technically, the

calculation of electrostatics consumes a significant portion of the computational expense of a simulation, thus limiting the simulation timescale and hence the sampling available to us.

For the non-ionic surfactants, linear polyethyleneglycol (PEG)-alkane diblock copolymers were chosen, denoted by C_xE_y where 'x' is the number of carbons in the hydrophobic alkane tail and 'y' is the number of ethylene glycol units in the hydrophilic head block. It should be noted that these surfactants have an extended as opposed to a compact head group (13). A linear alkane (heptane) is used for the oil phase. The NP sizes in the simulations presented here are in the range of 5.6 Å – 20.0 Å in radius.

Simulations were carried out in MPDyn (14) under isothermal-isobaric conditions, using a Nosé-Hoover thermostat (15), at 300.15 K, and an Andersen barostat (16), at 0.1 MPa, respectively. The reversible RESPA (17) algorithm was applied with a timestep of 20 fs for long ranged interactions, and a 2 fs timestep for all other interactions. Simulation box sizes were varied as necessary, with a typical unit cell side length of 100–150 Å.

All the simulated systems contained oil and water. Under constant composition, pressure, and temperature (NPT) conditions the system evolves to lower the Gibbs free energy, resulting in a phase separated box of oil and water corresponding to the minimum oil/water interfacial area, and hence the minimum free energy. These systems model oil/water interfaces of negligible curvature with respect to the dimensions of the individual NPs and surfactant molecules. Therefore, our results may be valid for macroscopically planar systems such as the water/toluene systems studied by Wang *et al.* (18), and also for oil/water emulsions where the droplet size is sufficiently large that the droplet boundary is essentially planar on the simulated length scale. An example of a simulation box is given in Figure 1, which shows the system components while also illustrating the periodic boundary image convention used in the simulations. The use of periodic boundaries maintains the solvent environment at the edges of the simulation box and allows for the representation of an extended oil/water interface without using an excessively large box size (19).

The interactions among the components must be specified to carry out simulations. This, and the representation of the species, are collectively known as the 'force field'. The representation we have used for this study is a coarse-grained (CG) force field where one CG 'bead' is representative of several atoms. For many areas of study this is an invaluable approach when the focus is on collective phenomena resulting from multitudes of molecules (20). By avoiding the complexity of calculating atomic movements and interactions CG simulations can attain high computational efficiency, and hence are able to simulate larger systems for longer timescales compared to fully atomistic simulations. In principle, the effect of atomic interactions are included in coarse grained force fields, *i.e.*, the interactions between two CG beads should be the ensemble averaged interaction due to all the atoms those beads represent. For example, two CG water beads do not form hydrogen bonds (because they do not contain explicit hydrogen atoms), but should account for the additional strength of interaction between water molecules due to hydrogen bonds. However, because CG approaches essential discard fine detail it is critical to apply this technique in

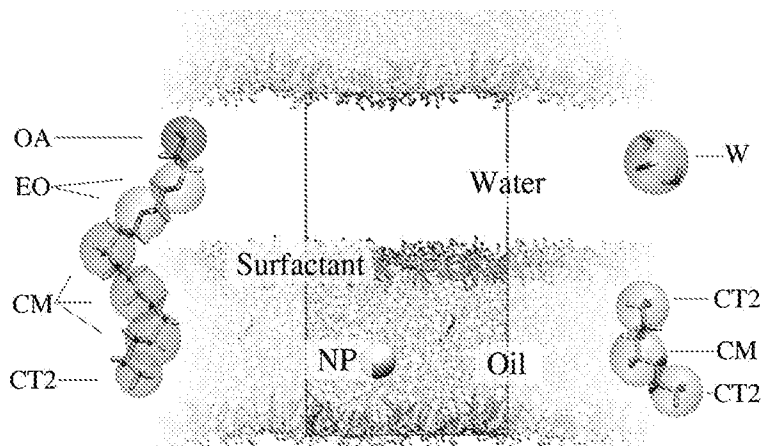


Figure 1. A side view of a representative simulation box comprising water (not shown), oil, surfactant and a single nanoparticle. The rectangular box designates the unit cell, while the periodic images are also shown. Due to the periodic image convention each simulation box contains two oil/water interfaces, which are perpendicular to the plane of the page in this example. To the left and right of the simulation box, the coarse-grained molecular representation (transparent spheres and bead labels) is superimposed on the atomistic representation (stick model).

systems where the atomistic interactions are not crucial to the phenomena under investigation (20). In this study we are investigating a wide range of systems in a qualitative manner, hence a strong argument can be made for the use of a CG model since it is not clear what additional knowledge could be gained through using a fully atomistic force field.

For the soft components (water, heptane and surfactant) the coarse-grained force field of Shinoda was used (21). This force field has been shown to accurately predict the phase behavior of PEG-alkane surfactants, and also the properties of oil/water systems including, most critically, the interfacial tension. Bond stretching is modeled through a harmonic potential, $U_{\text{bond}}(r) = k_b(r - r_e)^2$, where k_b is the bond force constant, r the separation between two covalently bound beads, and r_e their equilibrium separation. Bond bending is also modeled through a harmonic potential, $U_{\text{bend}}(\theta) = k_\theta(\theta - \theta_0)^2$, where k_θ is the force constant, θ the instantaneous angle between the three beads involved in a bond angle, and θ_0 the equilibrium angle. The relevant parameters used are given in Tables 1 and 2. Since the components we are using are uncharged, the non-bonded interactions comprise exclusively dispersive interactions which are modeled through the Lennard-Jones function,

$$U_{\text{LJ}}(r) = B \times \epsilon \left\{ \left(\frac{\sigma}{r} \right)^m - \left(\frac{\sigma}{r} \right)^n \right\} \quad (1)$$

Table 1. Force field parameters for bond stretching

	k_b kcal mol ⁻¹ Å ⁻²	r_e Å
CT2-CM	9.00	3.13
CM-CM	6.16	3.64
CM-EO	7.10	3.56
EO-EO	4.90	3.28
EO-OA	15.00	2.79

Table 2. Force field parameters for bond bending

	k_θ kcal mol ⁻¹ deg ⁻²	θ_0 deg
CT2-CM-CT2	1.70	173.0
CT2-CM-CM	1.60	172.0
CM-CM-CM	1.19	173.0
CM-CM-EO	1.50	172.0
CM-EO-EO	3.20	146.0
EO-EO-EO	3.40	132.0
EO-EO-OA	3.00	131.0

where σ is the exclusion volume, and m , n and B are chosen such that (1) $-\epsilon$ is the minimum of the potential profile, and (2) $U_{LJ}(\sigma) = 0$. Different choices for the integer powers m and n correspond to interaction potentials of different stiffness. The parameters are specific for each pair of interacting beads and are given in Table 3.

The representation of the NP and its interaction with the soft system components is based on a mean field approximation where the NP is modeled as a continuum solid sphere with a uniform interaction site density (22) in analogy to Hamaker's treatment of colloidal particles (23). The total interaction of the NP with another entity is found by integrating the site-site interaction over the volume of the NP. Hence, the interaction is governed by two parameters apart from particle geometry; (1) the density of interaction sites in the NP, ρ , and (2) the interaction strength parameter, ϵ , between sites on the NP and those on the interacting body. The ρ value chosen was that of graphitic carbon at 0.113 Å⁻³. The ϵ values for the interaction with oil were taken directly from fully-atomistic simulation data (22), while the NP-water interaction strength, ϵ_{NP-W} , is iteratively adjusted to obtain the desired hydrophobicity, for example, to match the experimental contact angle of a water droplet on a graphene surface (24). For this study a base value for ϵ_{NP-W} was taken as 0.596 kcal mol⁻¹, which for a NP of 10.0 Å radius corresponds to a slightly hydrophobic particle. During this chapter the set of ϵ values for the NP interaction with the all the different beads which make up the two solvents are collectively indicated by ϵ_{Solv} . It should

Table 3. Force field parameters for non-bonded interactions

	CT2		CM		EO		OA		W	
	σ	ϵ	σ	ϵ	σ	ϵ	σ	ϵ	σ	ϵ
W	4.296	0.290	4.438	0.340	4.310	0.570	3.950	0.700	4.371	0.895
OA	3.840	0.380	4.274	0.377	3.890	0.440	3.713	0.4491		
EO	4.140	0.370	4.274	0.377	4.250	0.405				
CM	4.364	0.362	4.506	0.420						
CT2	4.221	0.312								

The σ and ϵ parameters for pairs of interacting types of CG beads given in units of Å and kcal mol⁻¹, respectively. For interactions involving water, m=12 and n=4 while for all other interactions m=9 and n=6.

be noted that the curvature of the NP-water interface (and hence the NP size) also strongly affects the NP hydrophobicity/hydrophilicity (25).

For the interaction between two NPs the same approach is used. The only difference is that the total interaction is found through integrating over the volumes of both NPs. The interaction strength between two interaction sites on different particles, ϵ_{NP-NP} , is 0.070 kcal mol⁻¹, which is the value for graphitic carbon.

Unfunctionalized NPs at Oil/Water Interfaces

In this section we discuss the ability of unfunctionalized NPs to lower the oil/water surface energy, beginning with the conceptual difference of NPs compared to molecular surface active agents (surfactants).

Interfacial Behavior of Surfactants versus Nanoparticles

For an isothermal-isobaric system (NPT ensemble), the interfacial localization of any discrete species is determined by the change in Gibbs free energy resulting from its adsorption to the interface (3). The excess free energy for an oil/water interface can be given as,

$$G = A_{ow} \gamma_{ow} \quad (2)$$

where A_{ow} is the surface area of the oil/water interface and γ_{ow} is the oil/water surface tension. The thermodynamic definition of the surface tension follows from the above equation,

$$\gamma_{ow} = \left(\frac{\partial G}{\partial A_{ow}} \right)_{N,P,T} \quad (3)$$

It is clear from Equation 2 that at the simplest level two factors affect the interfacial free energy, and hence that two mechanisms exist to lower this free energy. These two mechanisms are the ability of a species to reduce the oil/water contact area or to reduce the tension of the interface. The difference between

molecular surfactants versus NPs at oil/water interfaces is essentially based on this observation: surfactants lower γ_{ow} while NPs lower A_{ow} .

Some surfactants can lower the surface tension of the oil/water interface to the stability limit of zero. Beyond this limit addition of surfactants to the interface causes γ_{ow} to be lowered below zero, resulting in an instability which is released by an increase in the interfacial area corresponding to buckling or folding of the interface. In general the performance of surfactants in changing an interfacial property is measured through their efficiency and effectivity. In this context the efficiency of a surfactant is the equilibrium concentration of surfactant needed to lower the interfacial tension by a specific amount, and the effectivity is the maximum change the surfactant can induce in the interfacial tension (26). Due to their extensive use in industry, the behavior of many surfactant species (cationic, anionic, zwitterionic and neutral) at oil/water interfaces is well known. Many of the non-ionic surfactants, including those with polyethyleneglycol (PEG) heads, are effective at lowering the oil/water surface tension to zero. We refer any reader interested in learning more about the intrinsic activity of surfactants to the wide body of literature available on this subject (26, 27).

Conversely, theoretical treatments of NPs assume there is no change in the surface tension with adsorption of the NP to a fluid interface. The free energy change upon adsorption of a NP from the oil phase to the oil/water interface can be derived by considering the total surface excess free energy from all the interfaces present (3, 28). For a spherical particle of radius R , this leads to an expression as a function of η , the particle position measured from the interfacial plane (i.e. in the direction normal to the interface),

$$\Delta G(\eta) = \begin{cases} 0 & \eta < -R \\ 2\pi R^2(1 + \eta/R)(\gamma_{pw} - \gamma_{po}) - \gamma_{ow}\pi(R^2 - \eta^2) & -R \leq \eta \leq R \\ 4\pi R^2(\gamma_{pw} - \gamma_{po}) & \eta > R \end{cases} \quad (4)$$

Here the reference state ($\eta = -R$) corresponds to the particle being completely submerged in the oil phase and γ_{pw} and γ_{po} are the particle/water and particle/oil surface tensions, respectively. For the $-R \leq \eta \leq R$ range of $\Delta G(\eta)$, the first term is due to the gain or loss of particle/solvent surface area. The second term is the free energy change due to the removal of oil/water contact arising from the excluded volume of the NP. By considering the equilibrium condition (i.e. minimizing ΔG with respect to η), Young's equation can be derived,

$$\frac{\eta}{R} = \frac{\gamma_{po} - \gamma_{pw}}{\gamma_{ow}} \quad (5)$$

Here the quantity η/R is related to the equilibrium contact angle, θ , through $\cos \theta = \eta/R$, which is an experimental observable (29).

Some thermodynamic approaches suggest that accumulation of any solute at a fluid interface results in a lowering of the fluid/fluid interfacial tension (30), but this is at odds with both experimental and computational results which often show

the surface tension of fluid interfaces does not change upon particle adsorption (6, 7).

Transfer Free Energy Profile of Individual NPs

From molecular dynamics simulations the free energy profiles of NPs in the vicinity of an oil/water interface can be determined using the method of thermodynamic integration (31), in which a series of simulations are run varying the position η of the NP. In each simulation, η is kept constant through application of a harmonic biasing potential, from which the force of constraint is tracked. The mean value of the force of constraint for each simulation can be integrated with respect to η to obtain the free energy profile, $\Delta G(\eta)$ (32).

The transfer free energy profiles of two individual NPs at a heptane/water interface are shown in Figure 2. The general features predicted by Equation 4 are clearly visible, where $\Delta G(\eta)$ shows a parabolic minimum close to the interface ($\eta = 0$). The stability of the NP at the interface is seen to increase with particle size, in line with Equation 2 which predicts this stability increase to scale as R^2 . This is seen experimentally in polydisperse NPs at fluid interfaces, where the larger NPs displace the smaller NPs over time (33). Polydispersity can also lead to phase separation of the NPs into small islands at the fluid interface.

Dimerization Free Energy Profile of NPs Localized at the Interface

The spatial organization of NPs at fluid interfaces is a problem given much attention due to the implications born to many industrial and commercial fields (3, 34). An exhaustive survey of this topic is beyond the scope of this chapter, but conventional approaches to treat aggregation behavior are based on the Derjaguin-Landau-Verwey-Overbeek (DLVO) theory (3). DLVO theory treats charged particles in electrolyte solution by decomposing the net interaction between particles into an electrostatic double-layer repulsion and a dispersive attraction. Adoption of this theory to interfacial systems requires modifying the contributions to account for particle immersion in media of different permittivity and the distribution of charges which accompanies this (3). Furthermore, treatment of particle interactions at the interface needs to address phenomena not seen in the bulk such as capillary forces.

The work we have carried out is on small uncharged NPs and hence the forces due directly or indirectly to electrostatics and gravity are avoided. In this section we focus on the dimerization free energy of NPs at an oil/water interface evaluated through MD simulation data and we attempt to give a conceptual reasoning for the observed features.

In an ideal gas reference state the NPs, interacting only through dispersion forces, show a simple form for their interaction free energy as a function of their separation. A single minimum exists corresponding to the physical contact of the particles. Separation values less than the minimum are strongly disfavored due to steric overlap.

When the NPs are localized at an oil/water interface, their mutual interaction is more complicated (35) as seen in the dimerization free energy profiles shown

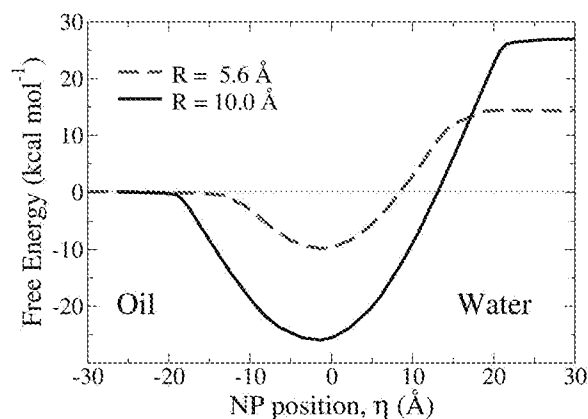


Figure 2. Transfer free energy profiles of two unfunctionalized NPs, from a reference state in bulk heptane to a bulk water environment. These NPs are considered hydrophobic due to their preference to solvate in the oil phase. Note that the active η range is broader than predicted by Equation 2 due to dispersion forces.

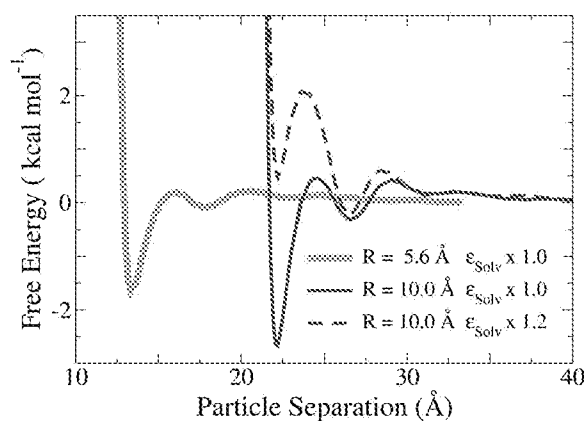


Figure 3. Dimerization free energy profiles of three pairs of unfunctionalized NPs as a function of their interparticle separation at an oil/water interface. The increase in interaction energy with particle size is seen between the two profiles shown in solid lines (radius 5.6 Å versus radius 10.0 Å; $\epsilon_{NP-W} = 0.596 \text{ kcal mol}^{-1}$). The effect of solvation is seen through the two radius 10.0 Å profiles.

in Figure 3. Dimerization profiles for two sizes of NPs were calculated using the previously described techniques, namely constrained molecular dynamics and thermodynamic integration of the mean force of constraint with respect to the interparticle separation.

The profiles in Figure 3 show the undulations in free energy which arise due to the solvation of the NPs at the interface. Individual particles tend to order solvent molecules in layers around them. The dimerization of two such particles involves the restructuring and desolvation of these solvent layers giving

the undulations in the dimerization free energy profile. Solvent interaction with the particle diminishes with distance and hence the undulations in the profile decrease in magnitude the further away the particles are from one another. Conceptually the disruption of a solvation shell entails an enthalpic loss of the solvent-particle interaction which is countered by the enthalpic gain of solvent-solvent interactions, particle-particle interaction and an entropic gain through disruption of the ordered solvent layer.

The scaling of interaction magnitude with particle size is also exemplified in Figure 3 (profiles in solid lines). Here the deepening of the free energy minimum at particle contact is clear, as well as the increase in the amplitude of undulations caused by solvent restructuring. Both these effects are caused by size (curvature) dependence of the NP/solvent and NP/NP interactions.

The dimerization free energy profiles of Figure 3 also show the effect of increasing the particle-solvent interaction strength. Through scaling ϵ_{Solv} by a factor of 1.2 the global minimum of the free energy profile can be shifted from being at close-contact (Figure 3, thin solid line) to a minimum corresponding to a solvent layer separating the two particles (Figure 3, dashed line). This is thought to be due to the particle-solvent enthalpic contribution overtaking the contributions which stabilize the system when the particles are in contact.

Organization of NPs at an Oil/Water Interface

The dimerization profiles shown Figure 3 are for two particles at an oil/water interface. However, the behavior of a NP in the presence of several others (localized at an oil/water interface) depends on the relative positions of all particles within their effective interaction range. Hence, predicting the two-dimensional spatial organization of NPs is a challenging task. Although the mutual interaction of particles is a manifold landscape it can be expected that there is a strong correlation between the features of the dimerization free energy profile and the overall interfacial structure. From simulations of different NPs at an oil/water interface we observed this relationship as shown in Figure 4. Specifically, simulations were carried out for the three types of NPs shown in the dimerization free energy profiles of Figure 3 and the resulting 2D structures are shown in Figure 4. As expected from the dimerization free energy profiles the particles with unscaled ϵ_{Solv} values form clusters with the particles in contact with one another. The radius 10.0 Å NPs form extended close-packed clusters while the radius 5.6 Å particles form smaller clusters. This may be due to the differences in free energy at particle contact which for the radius 5.6 Å particles is comparable to the thermal energy and hence subject to thermal fluctuations.

The effect of increasing the solvent interaction strength is also seen in Figure 4 where the radius 10.0 Å with ϵ_{Solv} scaled by 1.2 shows no NP clustering. This behavior is commensurate with the largely repulsive dimerization profile of Figure 3.

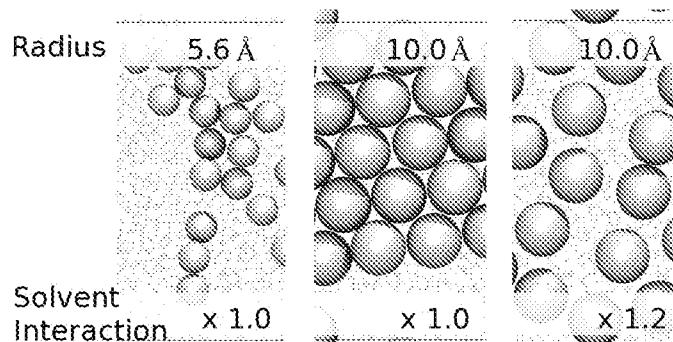


Figure 4. Equilibrium structure of NPs localized at an oil/water interface. Radius 5.6 Å particles (left) form small clusters while 10.0 Å radius NPs (center) form extended close packed structures. By increasing the particle-solvent interaction strength by a factor of 1.2 (right) the two-dimensional spatial organization of the radius 10.0 Å NPs is completely different.

Synergistic Interactions of Surfactants and NPs at Oil/Water Interfaces

The co-existence of surfactants and NPs can be broadly classified into two categories based on their interaction; (1) NPs in the presence of free surfactants; (2) chemically adsorbed surfactants.

First we consider NPs in the presence of free surfactants. At low coverage of surfactants ($\sim 65 \text{ \AA}^2$ per surfactant) and NPs ($\sim 651 \text{ \AA}^2$ per NP) both species are predominantly found at the interface. Representative systems are shown in Figure 5, for 10.0 Å radius particles with different ϵ_{solv} values.

Previous simulation studies have shown that C_{12}E_3 surfactants are successful at lowering the oil/water surface tension, γ_{ow} , to zero at a surface concentration of $\sim 32.5 \text{ \AA}^2$ per surfactant. For a simulation cell of surface area $125 \text{ \AA} \times 125 \text{ \AA}$ this corresponds to ~ 480 surfactants. To investigate how the presence of NPs affects the behavior of the surfactants a system of the above surface area was prepared with half the maximum coverage, i.e. 240 C_{12}E_3 molecules localized at each oil/water interface. In addition to the surfactants, varying numbers of NPs are positioned at the interface. The systems are allowed to equilibrate for 10 ns, after which data is collected from longer equilibrium simulations. Conformations of these systems after 50 ns are shown in Figure 6.

From Figure 6, it is clear that the surfactants are sparingly soluble in oil. It is also clear that at higher NP concentrations the NP interfacial distribution is shifted towards the oil phase and some NPs are dislodged from the interface towards the oil phase. To further discuss this trend let us quantify the effectivity of the surfactants through their effect on γ_{ow} , the oil/water interfacial tension.

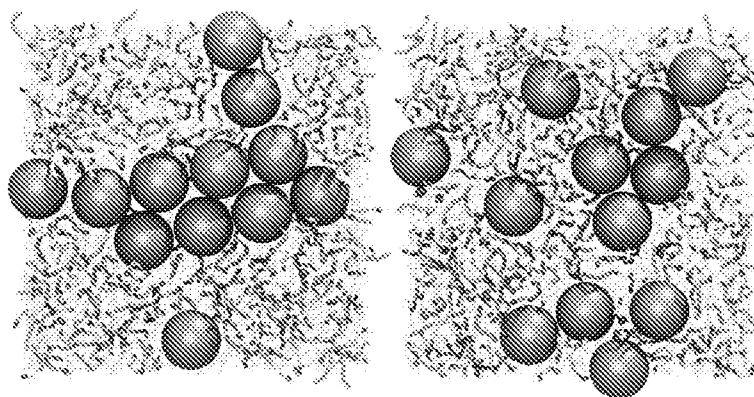


Figure 5. (left) 24 radius 10.0 Å particles with 240 $C_{12}E_3$ surfactants at an oil/water interface. (right) The same system with the particle-solvent interactions scaled by a factor of 1.2.

Surface Tension Measurements and Cooperativity Between NPs and Surfactants

The synergy of surfactants and NPs in lowering the surface tension of the oil/water interface has received interest recently (6, 7, 36, 37) and research into this phenomena is ongoing. However, most of the observed synergy is caused by electrostatic interactions between charged particles and ionic surfactants, whereas we report synergistic effects in systems of uncharged NPs and non-ionic surfactants.

Since both surfactants and NPs are localized at the oil/water interface some cooperativity in lowering the oil/water surface tension may be expected. A simple hypothesis is that NPs, through removal of oil/water contact, decrease the effective interfacial surface area over which the surfactants act. This would effectively lower γ_{ow} compared to when the same quantity of surfactants were acting on the interface in the absence of NPs.

The series of simulations shown in Figure 6 was designed to test this hypothesis. When localized at the interface, a single NP of radius 10 Å removes over 300 Å² of oil/water surface area. Therefore by using 24 NPs in a 125 Å × 125 Å surface area system, more than half of A_{ow} is effectively removed. If our hypothesis holds true throughout this composition range, the surface tension would be expected to show a monotone decrease to a final value of close to zero for the four systems of Figure 6. However, the actual change of γ_{ow} is given in Figure 7 and invalidates our hypothesis.

Initially, when no NPs are present, the system has a surface tension of 29.3 mN m⁻¹ which is roughly half of the pure oil/water surface tension of 50.1 mN m⁻¹. The surface tension drops upon addition of NPs, indicating that there is synergy between the two species at low NP concentrations. However, at higher concentrations the expected lowering of surface tension is not seen, and instead the surface tension plateaus at ~12 mN m⁻¹.

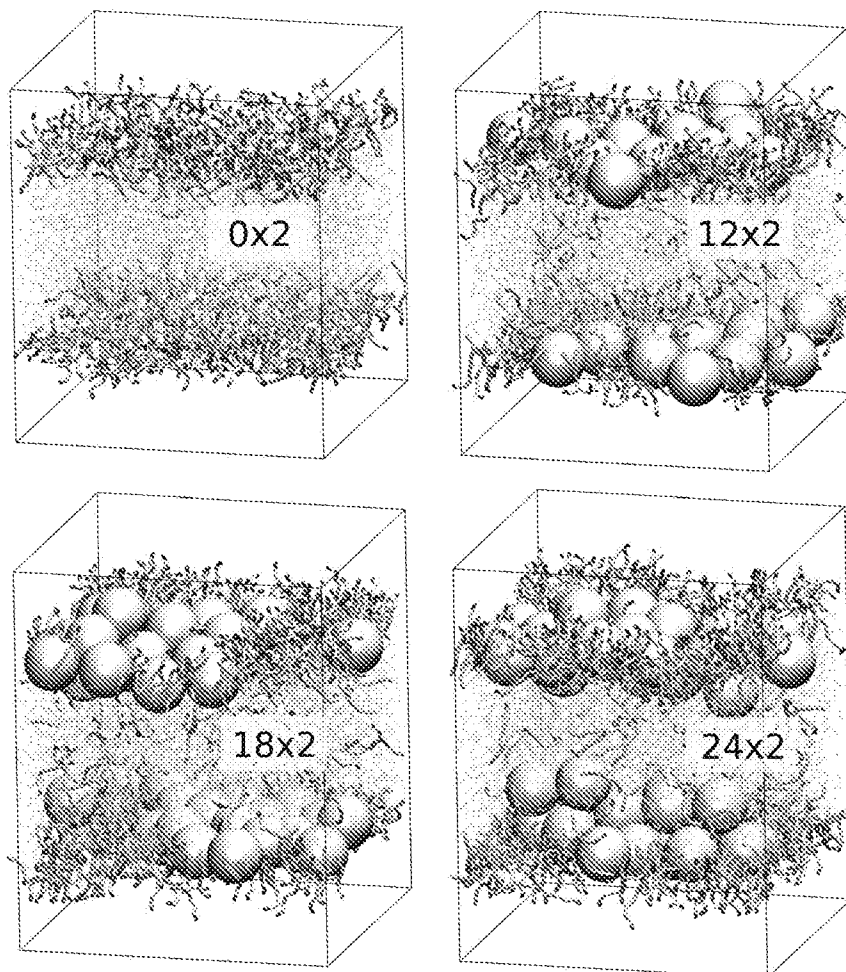


Figure 6. Snapshots of oil/water interfaces with varying numbers (labeled in each panel) of radius 10 Å NPs and 240 $C_{12}E_3$ surfactants. The $\times 2$ is used to indicate the presence of two interfaces of identical composition. The coloring scheme is identical to Figure 1.

These results can be rationalized by acknowledging that the localization of NPs at the interface is driven by the last term of Equation 4, $-\gamma_{ow}\pi(R^2 - \eta^2)$. Surfactants act to lower the value of γ_{ow} , decreasing the thermodynamic driving force for particle adsorption to the interface. Past a critical value of the oil/water surface tension, the excess interfacial free energy of the oil/water interface, $A_{ow}\gamma_{ow}$, is no longer the dominant factor and further localization of particles is not favorable. This is seen in Figure 6 where the equilibrium position of the NPs shifts towards the oil phase, and particles are also pushed into the oil phase.

If the NPs used in this study instead preferred water over oil (see Figure 2) we would expect the opposite behavior, namely that the NPs would be displaced towards the water phase upon addition of surfactants.

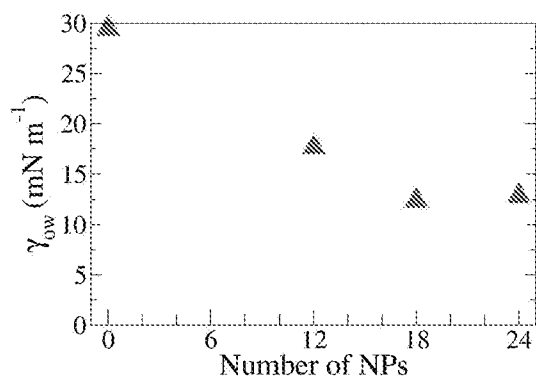


Figure 7. Oil/water interfacial tension for the systems shown in Figure 6. Initial addition of NPs lowers the γ_{ow} value although the synergistic effect diminishes with increasing numbers of NPs.

Surfactant Functionalized NPs

We now turn our attention to NPs functionalized with chemically absorbed surfactants. Organic ligands are often used to functionalize NPs to improve their colloidal stability, chemical stability, and interfacial activity (38). An example is the use of (mercaptoundecyl)tetra(ethylene glycol) ether functionalized gold nanoparticles to stabilize oil in water emulsions (39). It should be noted that this is a commercially available product, and is identical to the C_xE_y (with $x = 12$, $y = 4$) class of surfactants, except for an additional thiol moiety at the alkane terminus.

Ongoing MD simulation studies have shown the dramatic changes such chemical functionalization has on the interfacial activity and the dimerization free energy profile of NPs. For example, consider the 5.6 Å radius NP shown in Figure 2, which shows a free energy minimum of ~ 10.0 kcal mol⁻¹. Attachment of 20 $C_{12}E_2$ surfactants to this particle lowers the interfacial binding free energy to ~ 60 kcal mol⁻¹. Furthermore, preliminary results indicate that the dimerization free energy of NPs is also changed significantly. For the 10 Å radius particle, addition of even 10 $C_{12}E_3$ surfactants removes the attractive well, and the free energy of dimerization becomes completely repulsive.

The focus of this section is on simulations carried out on a NP of core radius 5.6 Å and $\epsilon_{NP-W} = 0.378$ kcal mol⁻¹, with 20 bound $C_{12}E_2$ ligands. Emphasis is given to the role the surfactants play in shape deformations of the NP in the vicinity of an oil/water interface. A parameter for quantifying the tendency to deform is introduced as δ , the system deformability.

In the beginning of the chapter a simple theoretical model of the energetics of NPs at oil/water interfaces was presented. Some deficiencies of this theory are known, but a critical assumption made in its derivation is the ideal spherical shape of the NP itself. The flexibility of the surface functionalizing ligands violates this assumption (here we consider the NP to be the composite of the core and the functionalizing ligands). For larger cores (e.g. micron sized particles) the deformable layer is negligible and the assumption of spherical geometry may be accurate. However the importance of the deformable layer increases with smaller

NP core sizes, and could play an important role in some cases in determining the behavior of NPs at fluid interfaces (32).

Surfactant-Solvent Interactions and Preferential Orientation of Surfactant Ligands Functionalizing a NP Core

For the 5.6 Å particle functionalized with 20 C₁₂E₂ ligands considered here, the core is of ~1.1 nm diameter and the surfactant chains are of fully extended length ~1.5 nm, i.e., the two components are of similar length scales. Simulations of the particle at different positions relative to an oil/water interface were carried out. Representative images from these simulations are shown in Figure 8 from which it is clear that the surfactants strongly interact with the interface. The preferential orientations of the surfactants cause shape deformations of the NP as seen in Figure 8.

The preferred orientation of the surfactants is quantified by the angle distributions shown in Figure 9. At η values where the NP is in a bulk solvent environment corresponding to the first and last panels in Figure 8, there is no preferred orientation of the surfactant chains and hence uniform distributions are seen in Figure 9. Pronounced peaks are visible at η positions where the surfactants can interact with the interface (bottom left panel of Figure 9). It should be noted that Equation 4 predicts changes in ΔG only between $-R \leq \eta \leq R$ and at larger η positions the particle is completely solvated in bulk solvent. However, dispersive interactions of the deformable coating of the NP with the interface broadens the η range over which the free energy varies.

All the observed results can be explained through the preferred solvation environments of the PEG and alkane segments of the surfactants. When the NP is deep within the heptane phase, the surfactants do not need to protect the surface of the core (since Figure 2 established that the core prefers oil over water) and hence show extended conformations, swelling the ligand corona of the NP. At η values within dispersive interaction range of the interface, the PEG units are attracted towards the water phase resulting in preferred orientations of the surfactant chains at the interface. At the interface the surfactants create an annular ring with the PEG segment curling into the water phase (see the middle panel of Figure 8). Similar behaviors can be observed in the water phase ($\eta > 0$), but here the surfactants protect the high-energy NP/water surface by collapsing onto the NP core.

The extent of swelling of the surfactant layer in oil versus water is important because it is indicative of the conformational freedom of the surfactants with respect to the NP core and hence the susceptibility of the NP to deform in shape. To measure the extension of the ligands from the NP core the radius of gyration, R_g , can be used. In this context R_g can be taken as,

$$R_g^2 = \frac{1}{N} \left\langle \sum_{i=1}^N (r_i - r_{NP})^2 \right\rangle \quad (6)$$

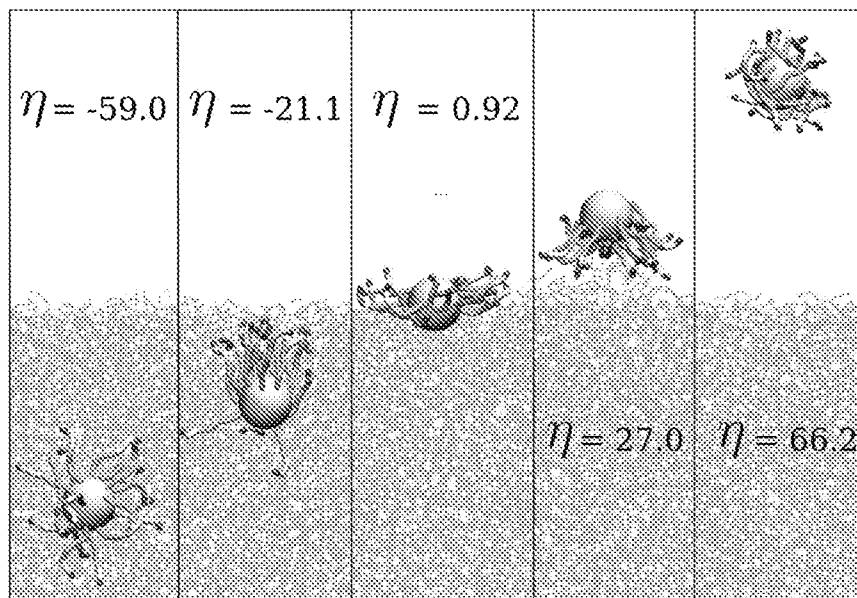


Figure 8. Snapshots of a core radius 5.6 Å NP functionalized with 20 C₁₂E₂ ligands in the vicinity of a planar oil/water interface. The surfactants adopt conformations in which the PEG block is close to water and the alkane block is close to heptane. These preferential orientations and conformations cause a position dependent deformation of the NP shape. η values are given in units of Å.

where r_i is the position of the i^{th} surfactant bead, r_{NP} is the nanoparticle core position and N the total number of surfactant beads.

The radius of gyration for the functionalized NP in oil, $R_g(\text{o})$, and water, $R_g(\text{w})$, are 16.00 Å and 13.50 Å respectively. The values for $R_g(\text{o})$ and $R_g(\text{w})$ for other selected NP systems are given in Table 4. It is clear from the table that in all cases the NP is swollen to a greater extent in oil than in water.

Deformability

As stated previously, the difference of the radius of gyration values in the two bulk solvent phases is related to the susceptibility of the particle to deform according to its environment. Using this information, a dimensionless parameter, the system deformability (δ) can be defined,

$$\delta = \frac{C|R_g(\text{o}) - R_g(\text{w})|}{R_g(\text{w}) + R_g(\text{o})} \quad (7)$$

where C is a scaling factor taken as 20 (to bring the value to a convenient scale). The δ value for the NP studied in the previous section is 1.69. Table 4 also includes δ values for other NP systems, in order to see some trends in deformability. The deformability increases with the ability of the particle to change shape, based

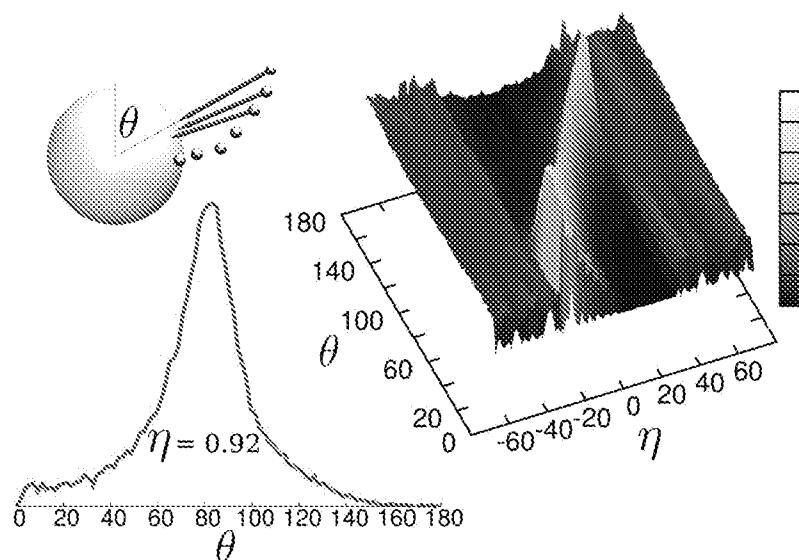


Figure 9. Angle distribution plots of 20 $C_{12}E_2$ surfactant ligands chemisorbed to a 5.6 Å radius NP core as a function of the interfacial position η of the NP (in units of Å). The angle between the oil/water interfacial normal vector and each NP center to surfactant bead vector (shown in the top left panel) was tabulated to obtain orientational distributions for specific values of η (bottom left). Plotting these distributions versus η produces the multidimensional graph shown in the top right panel.

on the ratio of the change in the radius of gyration values (numerator) to the average size of the particle (denominator). This parameter captures the effect of (1) increased density of surfactant coverage, which tends to lock the surfactants and hence lower the numerator, (2) changes in surfactant composition, which affects the R_g values, and (3) the ratio of the average extension of the surfactants to the NP core size. A graphical illustration of different NP types and their corresponding deformability parameters is given in Figure 10.

Measures of the ‘softness’ of particles are important in a number of fields. It has been shown that the deformability of particles has an effect on their rheological (40) properties as well as their self-assembly properties (41). Other measures of softness exist, an example being the χ factor used by Whetten *et al.* (42). This quantity is simply the ratio of the fully extended length of the functionalizing molecule to the size of the rigid core, which is used to predict the three-dimensional packing patterns of particle assemblies. The importance of characterizing the softness of particles was asserted by Tsai (43) who suggested that for any medicinal application of NPs rigorous physical and chemical characterization of particle size and structure is necessary. In the same article the author articulates the need for ‘complementary, orthogonal methods’ for this characterization. The δ parameter calculated through molecular dynamics simulations as introduced above is a prime example as a valuable characteristic property of functionalized NPs.

Table 4. Radius of gyration values for surfactant functionalized NPs

System	NP Core Size* (Å)	Surfactant Ligand	Number of Ligands	$R_g(o)$ (Å)	$R_g(w)$ (Å)	δ
1	5.6	C ₁₂ E ₂	20	16.00	13.50	1.69
2	5.6	C ₁₂ E ₂	40	16.93	15.50	1.77
3	5.6	C ₁₂ E ₃	20	16.97	15.52	1.79
4	5.6	C ₁₂ E ₃	40	18.05	16.30	2.03
5	10.0	C ₁₂ E ₃	46	21.05	20.08	0.94
6	10.0	C ₁₂ E ₃	91	22.42	21.09	1.22
7	10.0	C ₁₂ E ₃	183	23.92	23.70	0.18
8	20.0	C ₆ E ₁	286	27.15	26.94	0.16
9	20.0	C ₁₂ E ₃	286	32.60	31.76	0.52
10	20.0	C ₁₈ E ₅	286	38.18	35.71	1.34

* other than system 1, for which $\epsilon_{NP-W} = 0.378 \text{ kcal mol}^{-1}$, all other NP cores (systems 2-10) considered in the table have an $\epsilon_{NP-W} = 0.596 \text{ kcal mol}^{-1}$

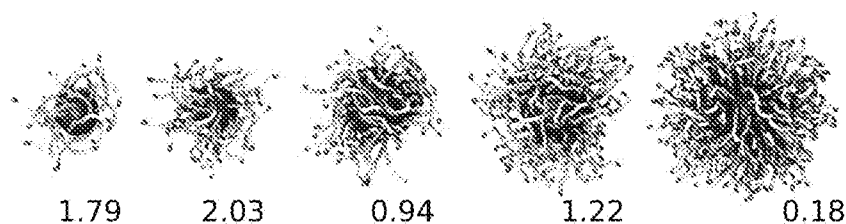


Figure 10. Selected NPs with different deformability (δ) values, shown below each NP image. From left to right the particles correspond to systems 3-7 of Table 4.

Conclusions

We have studied systems containing NPs and surfactants at oil/water interfaces using molecular dynamics computer simulations. We separately considered situations where the surfactants were free versus chemically absorbed to the NP core surface. It was found that at low surfactant and NP concentration, these species showed a synergistic effect in lowering the oil/water surface tension. However, as the effective area per surfactant is decreased the energetic drive for particle localization to the interface is severely attenuated. Studies of surfactant functionalized NPs showed that the interaction of the surfactants with the oil/water interface causes deformations in the NP shape. The ability of a particle to deform due to its environment was quantified using a deformability parameter δ . We hope to use this parameter in future studies of surfactant functionalized NPs to relate the surfactant layer properties to the properties of NP interfacial assemblies.

References

1. Pickering, S. U. *J. Chem. Soc.* **1907**, 91, 2001–2021.
2. Ramsden, W. *Proc. R. Soc. London, Ser. A* **1903**, 72, 156–164.
3. *Colloidal Particles at Liquid Interfaces*; Binks, B. P., Ed.; Cambridge University Press: New York, 2006.
4. *Colloids and Colloid Assemblies*; Caruso, F., Ed.; Wiley-VCH: Weinheim, 2004.
5. Day, L. In *An Encyclopaedia of the History of Technology*; McNeil, I., Ed.; Routledge: New York, 1990; pp 203–204.
6. Hunter, T. N.; Pugh, R. J.; Franks, G. V.; Jameson, G. J. *Adv. Colloid Interface Sci.* **2008**, 137, 57–81.
7. Binks, B. P. *Curr. Opin. Colloid Interface Sci.* **2002**, 7, 21–41.
8. Daniel, M. C.; Astruc, D. *Chem. Rev.* **2004**, 104, 293–346.
9. Murray, C. B.; Kagan, C. R.; Bawendi, M. G. *Annu. Rev. Mater. Sci.* **2000**, 30, 545–610.
10. Gupta, A. K.; Gupta, M. *Biomaterials* **2005**, 26, 3995–4021.
11. Russel, W.; Saville, D.; Schowalter, W. *Colloidal Dispersions*; Cambridge University Press: Cambridge, 1989.
12. Shevchenko, E. V.; Talapin, D. V.; Kotov, N. A.; O'Brien, S.; Murray, C. B. *Nature* **2006**, 439, 55–59.
13. Nagarajan, R.; Ruckenstein, E. *Langmuir* **1991**, 7, 2934–2965.
14. Shinoda, W.; Mikami, M. *J. Comput. Chem.* **2003**, 24, 920–930.
15. Hoover, W. G. *Phys. Rev.* **1985**, 31, 1695–1697.
16. Andersen, H. C. *J. Chem. Phys.* **1980**, 72, 2384–2393.
17. Tuckerman, M. E.; Berne, B. J.; Martyna, G. J. *J. Chem. Phys.* **1991**, 94, 6811–6815.
18. Wang, J.; Wang, D.; Sobal, N. S.; Giersig, M.; Jiang, M.; Mohwald, H. *Angew. Chem., Int. Ed.* **2006**, 45, 7963–7966.
19. Frenkel, D.; Smit, B. In *Understanding Molecular Simulation*; McNeil, I., Ed.; Academic Press: San Diego, 2002; p 34.
20. Müller, M.; Katsov, K.; Schick, M. *Phys. Rep.* **2006**, 434, 113–176.
21. Shinoda, W.; DeVane, R.; Klein, M. L. *Soft Matter* **2008**, 4, 2454–2462.
22. Kalescky, R. J. B.; Shinoda, W.; Moore, P. B.; Nielsen, S. O. *Langmuir* **2009**, 25, 1352–1359.
23. Hamaker, H. C. *Physica (Amsterdam)* **1937**, 4, 1058–1072.
24. Vázquez, U. O. M.; Shinoda, W.; Moore, P. B.; Nielsen, S. O. *J. Math. Chem.* **2009**, 45, 161–174.
25. Chiu, C.-c.; Moore, P. B.; Shinoda, W.; Nielsen, S. O. *J. Chem. Phys.* **2009**, 131, 244706.
26. Rosen, M. J. *Surfactants and Interfacial Phenomena*; John Wiley & Sons, Inc.: New York, 2004.
27. Lange, R. K. *Surfactants: A Practical Handbook*; Hanser Publishers: Munich, 1999.
28. Bresme, F.; Oettel, M. *J. Phys.: Condens. Matter* **2007**, 19, 413101–413133.
29. Murai, J.; Marukawa, T.; Mima, T.; Arai, S.; Sasaki, K.; Saka, H. *J. Mater. Sci.* **2006**, 41, 2723–2727.

30. Chandler, D. *Introduction to Modern Statistical Mechanics*; Oxford University Press: New York, 1987.
31. Frenkel, D.; Smit, B. *Understanding Molecular Simulation*; Academic Press: San Diego, 2002.
32. Ranatunga, R. J. K. U.; Kalescky, R. J. B.; Chiu, C.-c.; Nielsen, S. O. *J. Phys. Chem. C* **2010**, *114*, 12151–12157.
33. Lin, Y.; Boker, A.; Skaff, H.; Cookson, D.; Dinsmore, A. D.; Emrick, T.; Russell, T. P. *Langmuir* **2005**, *21*, 191–194.
34. Liang, Y.; Hilal, N.; Langston, P.; Starov, V. *Adv. Colloid Interface Sci.* **2007**, *134–135*, 151–166.
35. Bresme, F.; Lehle, H.; Oettel, M. *J. Chem. Phys.* **2009**, *130*, 214711.
36. Eskander, N. G.; Simovic, S.; Prestidge, C. A. *Phys. Chem. Chem. Phys.* **2007**, *9*, 6426–6434.
37. Luo, M.; Song, Y.; Dai, L. L. *Mol. Simul.* **2009**, *35*, 773–784.
38. Spertling, R. A.; Parak, W. J. *Philos. Trans. R. Soc., A* **2010**, *368*, 1333–1383.
39. Glogowski, E.; Tangirala, R.; He, J.; Russell, T. P.; Emrick, T. *Nano Lett.* **2007**, *7*, 389–393.
40. Zackrisson, M.; Stradner, P.; Schurtenberger, A.; Bergenholtz, H. *Phys. Rev. E* **2006**, *73*, 011408.
41. Landman, U.; Luedtke, W. D. *Faraday Discuss.* **2003**, *125*, 1–22.
42. Whetten, R. L.; Shafiqullin, M. N.; Khoury, J. T.; Schaaf, T. G.; Verzmar, I.; Wilkinson, A. *Acc. Chem. Res.* **1999**, *32*, 397–406.
43. Tsai, D.-H.; Zangmeister, R. A.; Pease, L. F., III; Tarlov, M. J.; Zachariah, M. R. *Langmuir* **2008**, *24*, 8483–8490.